Solid State Communications 175-176 (2013) 3–12

Contents lists available at ScienceDirect

Solid State Communications

journal homepage: www.elsevier.com/locate/ssc

Raman spectroscopy of twisted bilayer graphene

Ado Jorio [a,b,*], Luiz Gustavo Cançado [a,c]

[a] Departamento de Física, Universidade Federal de Minas Gerais, Belo Horizonte, MG 30123-970, Brazil
[b] Photonics Laboratory, ETH Zurich, CH-8093 Zurich, Switzerland
[c] Divisão de Metrologia de Materiais, Instituto Nacional de Metrologia, Qualidade e Tecnologia (INMETRO), Duque de Caxias, RJ 25250-020, Brazil

ARTICLE INFO

Article history:
Received 31 March 2013
Received in revised form
4 August 2013
Accepted 5 August 2013
Communicated by A.K. Sood
Available online 17 August 2013

Keywords:
A. Twisted bilayer graphene
D. van Hove singularities
D. Phonon dispersion
E. Raman spectroscopy

ABSTRACT

Twisted bilayer graphene (tBLG) is a two-graphene layers system with a mismatch angle θ between the two hexagonal structures. The interference between the two rotated layers generates a superlattice with a θ-dependent wavevector that gives rise to van Hove singularities in the electronic density of states and activates phonons in the interior of the graphene Brillouin zone. Here we review the use of Raman spectroscopy to study tBLG, exploring the θ-dependent effects, corroborated by independent microscopy analysis. The phonon frequencies give a Raman signature of the specific tBLG, while their linewidths provide a straightforward test for tBLG structural homogeneity. Rich resonance effects, including single and multiple-resonances, intra- and inter-valley scattering events make it possible to accurately measure the energy of superlattice-induced van Hove singularities in the electronic joint density of states, as well as the phonon dispersion relation in tBLG, including the layer breathing vibrational modes.

1. Introduction

When two identical periodic structures are superposed, a mismatch rotation angle between the structures generates interferences that gives rise to a superlattice. This effect is commonly observed in the surface of graphite, where the relative rotation of the graphene top layer with respect to the underlying layer generates a superlattice in scanning tunneling microscopy images, generally identified as a type of Moiré pattern [1]. With the rise of graphene [2], the prototype material for studying this phenomenon in a perfect two-dimensional solid state system is now available. Two perfectly oriented graphene layers on top of each other can form the so-called AA- or AB-stacking. By adding a twist angle θ between the layers, the AA- or AB-staking is lost and a superlattice structure is formed [3,4]. This system has been named the twisted bilayer graphene [3–5], abbreviated here as tBLG. With such ideal two-dimensional structure, high-resolution transmission electron microscopy (HRTEM) can now be used to directly image the Moiré pattern that is formed, as shown in Fig. 1 for a $\theta = 21^\circ$ tBLG [6].

The twist angle θ adds a new degree of freedom to the graphene system, generating several θ-dependent phenomena. On the electronic structure, the interference superlattice can generate seddle (M symmetry) points near the Fermi level [4,7,8] [see Fig. 2(a–c)]. In two dimensions the density of states (DOS) is logarithmic divergent at seddle points. Therefore, while monolayer graphene has a DOS linearly increasing when departing from the charge neutrality point [2], tBLG presents spiky van Hove singularities (vHs's) in the DOS, above and below the Fermi level [5]. The energy difference between these vHs's (E_{vHs}) can be tuned by changing θ, with important implications to the tBLG optoelectronics properties. For example, this phenomenon makes tBLG colored under an optical microscopy analysis, as already observed experimentally, with the color varying with θ [9,10]. This effect is explained theoretically considering the θ-dependence of the optical absorption, as shown in Fig. 2(d) [7].

On the phonon structure, the bilayer graphene is also a prototype system for studying the two-layers breathing mode, usually named ZO′ mode. These modes have been observed recently through non-linear combination modes in AB-stacked bilayer graphene [11]. In the tBLG, the superlattice generates a θ-dependent $\mathbf{q}(\theta)$ wavevector that activates phonons in the interior of the Brillouin zone, so that the ZO′ phonon branch can be probed directly in a first-order light scattering process [12]. This effect applies to the other phonon branches as well [12], so that the phonon dispersion of tBLG can be probed by first-order Raman scattering.

Raman spectroscopy is already established as a powerful tool to characterize the different types of carbon nanostructures, including graphene systems [13,14]. Relying on resonance effects, this technique was used to determine the structural dependence of the optical transition energies in carbon nanotubes, generating

* Corresponding author at: Departamento de Física, Universidade Federal de Minas Gerais, Belo Horizonte, MG 30123-970, Brazil. Tel.: +55 31 3409 6610; fax: +55 31 3409 5600.
E-mail addresses: adojorio@fisica.ufmg.br (A. Jorio), cancado@fisica.ufmg.br (L.G. Cançado).

0038-1098/$ - see front matter © 2013 Elsevier Ltd. All rights reserved.
http://dx.doi.org/10.1016/j.ssc.2013.08.008

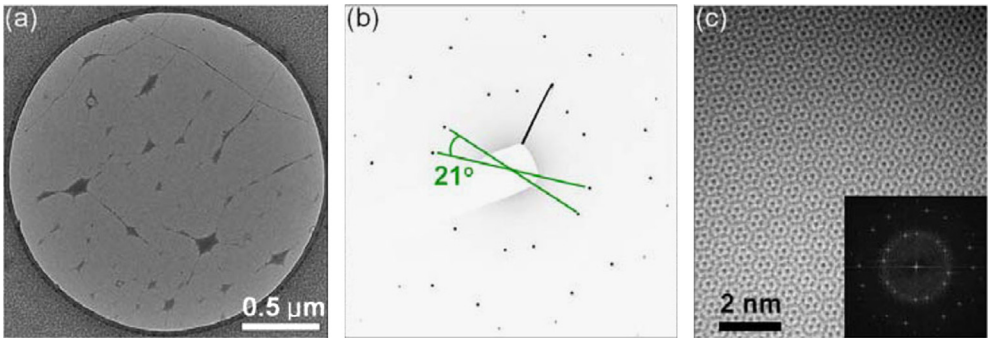

Fig. 1. (Color online) (a) Transmission electron microscopy (TEM) image of a tBLG in a TEM grid. (b) Electron diffraction pattern of the tBLG shown in (a). Two sets of hexagonal diffraction patterns are observed, rotated by 21° from each other. (c) High resolution TEM image of the same tBLG, showing the generated Moiré pattern. The inset shows a fast Fourier transform (FFT) of the image. From Ref. [6].

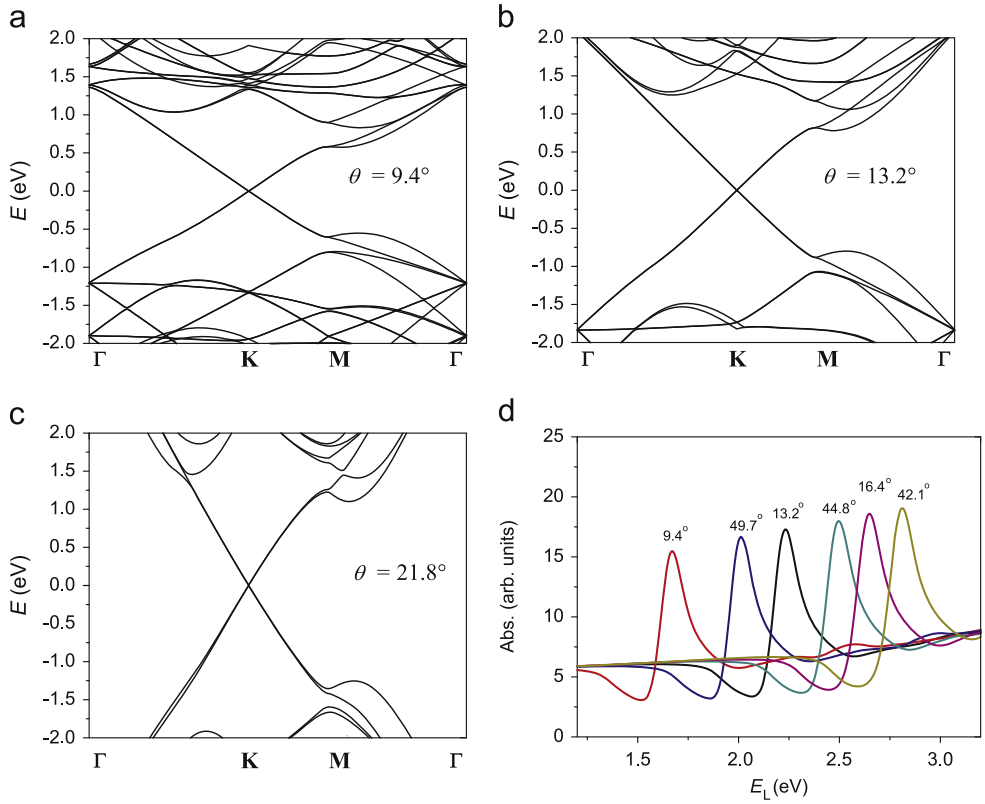

Fig. 2. (Color online) (a–c) Calculated electronic structure for three distinct tBLG. The rotation angles θ are indicated. (d) Calculated optical absorption spectra for six different values of θ, which are displayed near each respective absorption peak. From Ref. [7].

a signature for the chiral indices (n, m) [15–17]. Also due to resonance effects, the inelastic scattering of light could be used to map the phonon dispersion of graphene-related systems [18–20]. In general, Raman spectroscopy can always give a signature of the graphene-related structure, including structural or electronic deformations [13,14,21]. Here we review how this technique has been used to explore the θ-dependent effects in tBLG. This phenomenon has some similarities and differences with respect to the broadly studied double-resonance Raman effects in graphite and related materials, and these aspects will be explored here.

2. Structure—real and reciprocal space

Fig. 3(a) shows the schematics of a tBLG, with the red layer sitting on top of the blue layer. The top and bottom layers are rotated from each other by a generic angle θ, generating a periodic Moiré pattern. Fig. 3(b) shows this structure in the reciprocal space. $\mathbf{b}_1$ and $\mathbf{b}_2$ are the reciprocal lattice vectors of the bottom layer [blue layer in Fig. 3(a)]. These two reciprocal lattice vectors are given as $\mathbf{b}_1 = (2\pi/a)[(\sqrt{3}/3)\hat{\mathbf{k}}_x + \hat{\mathbf{k}}_y]$, and $\mathbf{b}_2 = (2\pi/a)[-(\sqrt{3}/3)\hat{\mathbf{k}}_x + \hat{\mathbf{k}}_y]$, where $a = 2.46$ Å is the lattice parameter of graphene, and $\hat{\mathbf{k}}_x$ and $\hat{\mathbf{k}}_y$ are the unit wavevectors [defined in Fig. 3(b)]. $\mathbf{b}_1'$ and $\mathbf{b}_2'$ [see Fig. 3(b)] are the reciprocal lattice vectors relative to the top layer [red layer in Fig. 3(a)], and they can be obtained by rotating the wavevectors $\mathbf{b}_1$ and $\mathbf{b}_2$, respectively, by an angle θ, giving

$$\mathbf{b}'_1(\theta) = \frac{2\pi}{\sqrt{3}a}[(\cos\theta - \sqrt{3}\sin\theta)\hat{\mathbf{k}}_x + (\sqrt{3}\cos\theta + \sin\theta)\hat{\mathbf{k}}_y], \quad (1)$$

$$\mathbf{b}'_2(\theta) = \frac{2\pi}{\sqrt{3}a}[(-\cos\theta - \sqrt{3}\sin\theta)\hat{\mathbf{k}}_x + (\sqrt{3}\cos\theta - \sin\theta)\hat{\mathbf{k}}_y]. \quad (2)$$

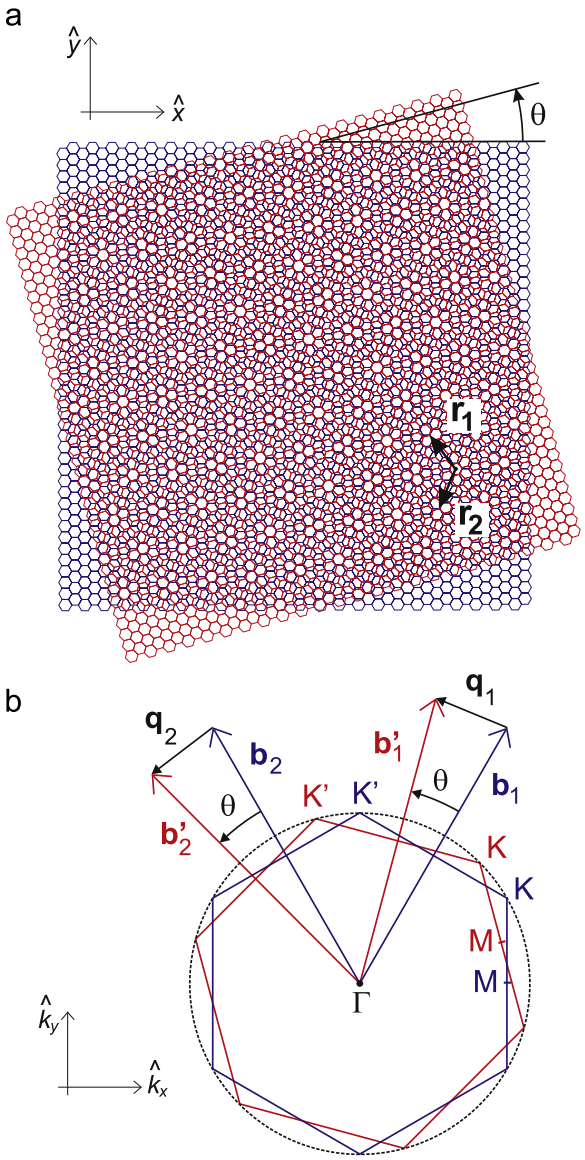

Fig. 3. (Color online) (a) Schematics of a rotationally stacked bilayer graphene, with the red layer sitting on the top of the blue layer. The top and bottom layers are rotated from each other by a generic angle θ starting from the AA-stacking, generating a periodic Moiré pattern. $\mathbf{r}_1$ and $\mathbf{r}_2$ are the direct lattice vectors defining the supercell, and $\hat{\mathbf{x}}$ and $\hat{\mathbf{y}}$ are the unit vectors in real space. (b) The 1st Brillouin zones of the stacked layers shown in panel (a). $\mathbf{b}_1$ and $\mathbf{b}_2$ are the reciprocal lattice vectors of the bottom layer [blue layer in part (a)]. $\mathbf{b}'_1$ and $\mathbf{b}'_2$ are the reciprocal lattice vectors of the top layer [red layer in part (a)]. $\hat{\mathbf{k}}_x$ and $\hat{\mathbf{k}}_y$ are the unit wavevectors. From Ref. [22].

As shown in Fig. 3(a), the mismatch between the two layers gives rise to a periodic superlattice, whose reciprocal rotational vectors $\mathbf{q}_1$ and $\mathbf{q}_2$ can be evaluated by taking the difference between the reciprocal vectors of the two lattices [22,23]. In terms of the unit vectors $\hat{\mathbf{k}}_x$ and $\hat{\mathbf{k}}_y$, these two reciprocal lattice vectors are given by $\mathbf{q}_1 = \mathbf{b}'_1 - \mathbf{b}_1$ and $\mathbf{q}_2 = \mathbf{b}'_2 - \mathbf{b}_2$, and the result is

$$\mathbf{q}_1(\theta) = \frac{2\pi}{\sqrt{3}a}\{[-(1-\cos\theta) - \sqrt{3}\sin\theta]\hat{\mathbf{k}}_x + [-\sqrt{3}(1-\cos\theta) + \sin\theta]\hat{\mathbf{k}}_y\}, \quad (3)$$

$$\mathbf{q}_2(\theta) = \frac{2\pi}{\sqrt{3}a}\{[(1-\cos\theta) - \sqrt{3}\sin\theta]\hat{\mathbf{k}}_x + [-\sqrt{3}(1-\cos\theta) - \sin\theta]\hat{\mathbf{k}}_y\}. \quad (4)$$

The graphene lattice has a 60° periodicity and is symmetrical around 30°, thus restricting our analysis for $0 \le \theta \le 30°$. For this reason, in the following discussion we drop the subscript indices 1 and 2, and we just use $\mathbf{q}(\theta)$.

The direct lattice vectors $\mathbf{r}_1$ and $\mathbf{r}_2$ defining the supercell can be obtained from the dot product $\mathbf{r}_i \cdot \mathbf{q}_j = 2\pi\delta_{ij}$, where $\{i,j\} = \{1,2\}$, and δ_{ij} is a Kronecker delta. The result is

$$\mathbf{r}_1(\theta) = -\frac{a}{4}[\sqrt{3} + \cot(\theta/2)]\hat{\mathbf{x}} - \frac{a}{4}[1 - \sqrt{3}\cot(\theta/2)]\hat{\mathbf{y}}, \quad (5)$$

and

$$\mathbf{r}_2(\theta) = \frac{a}{4}[\sqrt{3} - \cot(\theta/2)]\hat{\mathbf{x}} - \frac{a}{4}[1 + \sqrt{3}\cot(\theta/2)]\hat{\mathbf{y}}, \quad (6)$$

where $\hat{\mathbf{x}}$ and $\hat{\mathbf{y}}$ are the unit vectors in real space, as defined in Fig. 3(a). The vectors $\mathbf{r}_1$ and $\mathbf{r}_2$, calculated for that specific rotation angle θ, are also shown in Fig. 3(a). The modulus of the direct lattice vectors, $r_1 = r_2 = a/[2\sin(\theta/2)]$, determines the periodicity of the supercell [1,22,23].

Besides the Raman signature that will be discussed below, microscopy has been used to directly characterize the tBLG structures. TEM and electron diffraction have been used to assign the twist angle θ in different contributions in the literature [6,24,25], as illustrated in Fig. 1. Fig. 1(c) shows HRTEM image of a folded tBLG, while the inset shows a fast Fourier transform (FFT) analysis of the image. Both FFT analysis and electron diffraction [Fig. 1(b)] indicate a rotational angle of 21° between the two hexagonal structures [6]. In other works [7,22], lattice resolution atomic force microscopy (AFM) [26] has been used to assign the angle θ.

3. Production of tBLG

Twisted graphene layers occur naturally at the surface of crystalline graphite [1], so that the mechanical exfoliation method, broadly used to produce graphene samples, can generate such structures naturally. Accidental folding graphene into itself during the exfoliation procedure is also possible [27]. It has also been observed to occur in non-controlled way in graphene systems grown by chemical vapor deposition (CVD) [9,10,28]. Other techniques, such as washing exfoliated graphene with a water flux, can be applied to increase the yield of graphene structures folded into themselves [29].

A more sophisticated way to produce tBLG is by intentionally folding graphene using an AFM tip [7,22]. Fig. 4(a) shows a tapping mode AFM image of a monolayer graphene obtained from the micro-mechanical exfoliation process applied to graphite flakes, and deposited on top of a Si/SiO_2 substrate [7]. Defective lines were generated along a specific direction by scanning with the AFM tip several times over the same line [white arrows in Fig. 4(a)], applying a constant force. In sequence, the sample is scanned in the contact mode with the fast scanning direction parallel to the graphene edge. This process induces the folding of the graphene by cutting the sheet preferentially where the defect lines were induced, and then pushing it towards itself. The AFM image shown in Fig. 4(b) reveals three tBLGs produced by this method. The three folds were intentionally made along the same direction in order to produce three tBLGs with same twist angle θ. Lattice resolution AFM indicates a twist angle $\theta \simeq 26°$ [7]. Fig. 4(c) shows the Raman spectra obtained from the three tBLGs shown in panel (b). All three spectra exhibit the same new peak located at 1381 cm^{-1}, here named rotation-induced R band, which is the Raman signature of the $\theta \simeq 26°$ tBLG, as discussed in the next section.

4. The θ dependence of the Raman frequencies

Raman measurements performed on different tBLGs (different θ) are shown in Fig. 5 [12]. Besides the well-known Si features (at 225, 303, ~450 and 521 cm^{-1}) and the strong G band (at ~1584 cm^{-1}) from graphene, several new peaks are originated from the superlattice effect in tBLG, and these peaks are marked with ∗ in the spectra. The frequencies of these new rotation-induced R peaks change from sample to sample, and this change is indeed governed by θ.

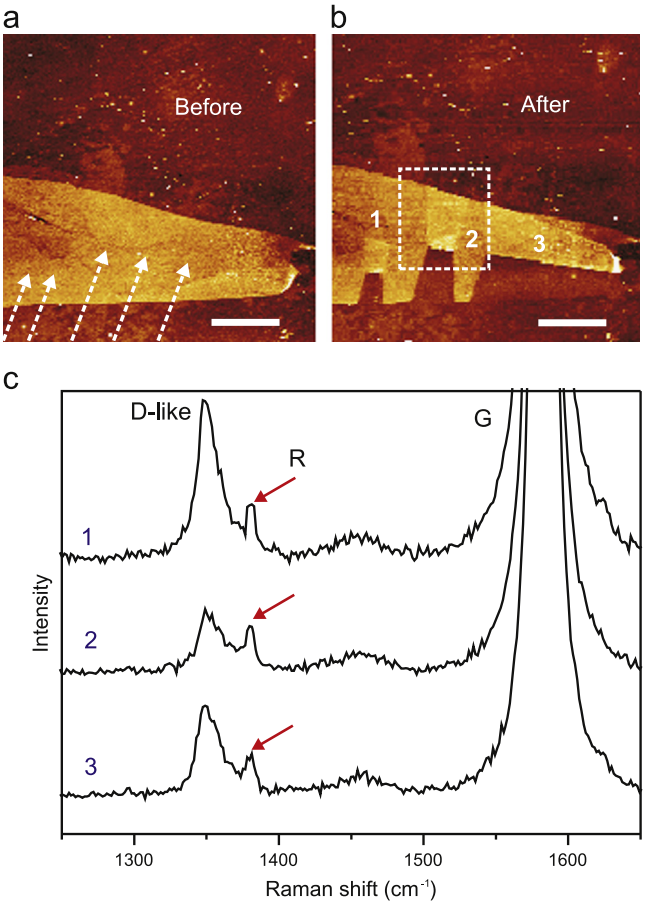

Fig. 4. (Color online) (a) AFM image of a monolayer graphene sitting on a Si/SiO_2 substrate. The white arrows indicate where defects were generated using AFM tip in contact mode. (b) Three tBLGs obtained by AFM folding. The scale bars in (a) and (b) denote 4 μm. (c) Raman spectra obtained from the three tBLGs shown in panel (b). The G band (~1584 cm^{-1}), the rotation-induced R band (~1381 cm^{-1}) and the "D-like" band are indicated. From Ref. [7].

Before explaining the θ dependence of the new R peaks in tBLG, Raman spectroscopy imaging has been used to prove that the R peaks come from tBLG. Fig. 6 shows two Raman images obtained from a tBLG produced by folding graphene into itself with an AFM tip [22]. In Fig. 6(a), the color scale renders the G band intensity. The G band signal can be detected from the whole graphene piece, and its intensity is twice in the folded region. This is expected, since the G band intensity is almost linearly proportional to the number of layers in few-layers graphene [30]. Fig. 6(b) shows the Raman intensity image of one of these new R peaks in tBLG, here the one centered at $\omega_R = 1625\ cm^{-1}$. The image shows that this peak can only be detected when the laser spot is focused on the folded region, i.e. on top of the tBLG.

The observation of these new R peaks in the Raman spectra of tBLG is due to the superlattice modulation that activates phonons in the interior of the Brillouin zone. The angle θ dictates the wavevector $\mathbf{q}(\theta)$ for this modulation, as defined in Eq. (3) [or Eq. (4)], so that the R peaks, marked with ∗ in Fig. 5, can be all mapped into the bilayer graphene phonon dispersion, by using the phonon wavevector $\mathbf{q}(\theta)$.

The exact assignment has to take into account that the direction of $\mathbf{q}(\theta)$ depends on θ. In Fig. 7, the arrows show the evolution of the wavevector $\mathbf{q}(\theta)$ [as defined in Eq. (3)], by varying θ between 0° and 30°. As an approximation, the assignment can be simplified by using the phonon dispersion curves in the high symmetry Γ–K direction. As shown in Fig. 7, the exact $\mathbf{q}(\theta)$ vector only departs significantly from the Γ–K direction when approaching the K point. Taking into account the isotropy of the phonon dispersion curves around and close to the K point, the R band frequency obtained from a sample with a twist angle θ can be approximated to the frequency of a phonon with wavenumber $q_{\Gamma\text{-K}}$ along the Γ–K direction. The $q_{\Gamma\text{-K}}$ component is indicated in Fig. 7 by the crossing (red diamonds) of the Γ–K line (dashed line) with the $\mathrm{K}-\mathbf{q}(\theta)$ equi-wavenumber contours (green arcs). The relation between $q_{\Gamma\text{-K}}$ and the twist angle θ can be obtained with simple trigonometry, and it is given by

$$q_{\Gamma\text{-K}} = \frac{4\pi}{3a}\left(1-\sqrt{7-2\sqrt{3}\,\sin\,\theta-6\,\cos\,\theta}\right). \tag{7}$$

The solid lines in Fig. 8(a) are the plots of the phonon frequencies of monolayer graphene as a function of $q_{\Gamma\text{-K}}$, taken from Ref. [31]. In Fig. 8(b), the solid lines show the same phonon dispersion curves, but with $q_{\Gamma\text{-K}}$ translated into θ, according to

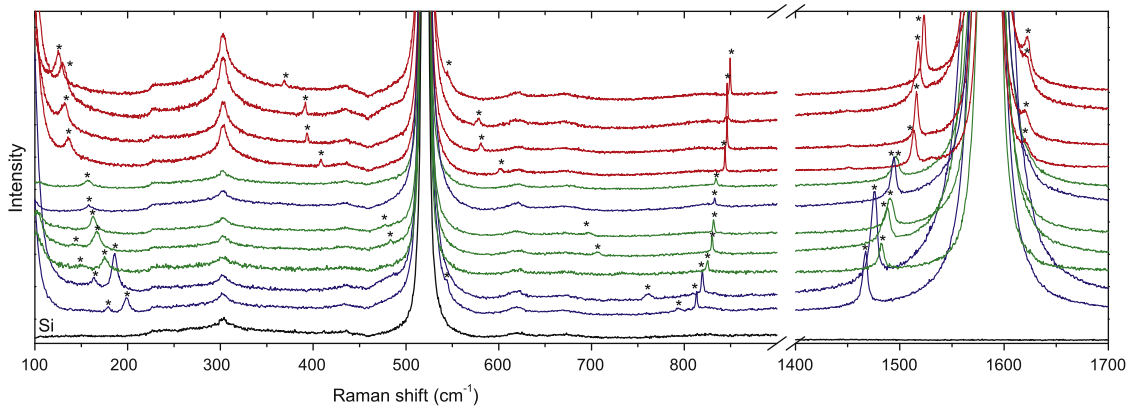

Fig. 5. (Color online) Raman spectra of tBLGs with different rotational angles sitting on a Si/SiO_2 substrate [12]. The tBLG samples were grown by chemical vapor deposition (CVD) at low pressures using methane as carbon source and copper foil as catalyst. The ∗ symbols point to the superlattice-induced Raman peaks (so-called R peaks) originated from tBLG. Curve coloring corresponds to the excitation laser energy used to acquire the spectra; red: $E_L = 1.96$ eV, green: $E_L = 2.41$ eV and blue: $E_L = 2.54$ eV; exception for the bottom (black) spectra ($E_L = 2.41$ eV), which is the Si substrate reference signal.

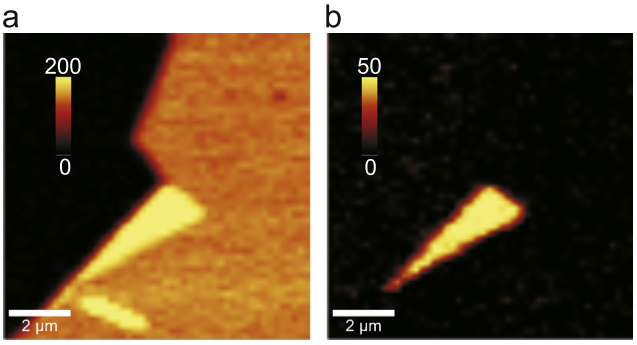

Fig. 6. (Color online) (a) G band intensity image obtained from a tBLG produced by folding graphene into itself with an AFM tip. (b) Raman intensity image of an R peak observed at $\sim 1625\ \mathrm{cm}^{-1}$. From Ref. [22].

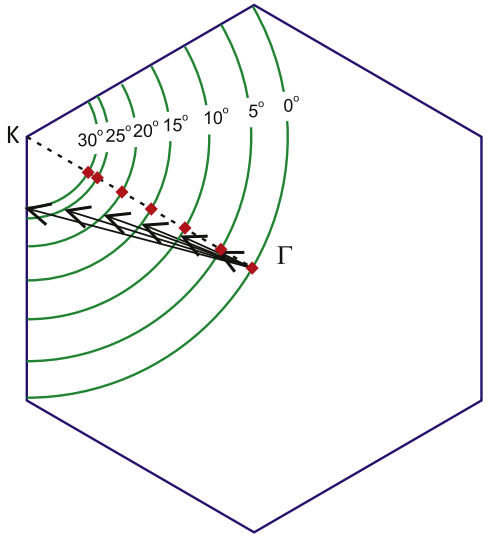

Fig. 7. (Color online) First Brillouin zone of graphene. The arrows show the evolution of the wavevector $\mathbf{q}(\theta)$ [as defined in Eq. (3)], by varying θ between 0° and 30° [12]. The circular arcs around the K point indicate equi-wavenumber contours measured from K, associated with specific values of θ indicated in the picture. Vectors pointing from Γ to the red diamonds would indicate the components $q_{\Gamma-\mathrm{K}}$ along the Γ–K direction.

Eq. (7). In both graphics, the ◇ and □ symbols correspond to the frequencies of the rotationally induced R peaks marked with ∗ in Fig. 5, demonstrating that all these features are indeed related to the phonon branches in tBLG [22]. The higher frequency peaks from tBLG have been named R and R′ peaks, in correlation to double-resonance defect-induced D and D′ bands [22]. Here we propose all these new peaks observed in tBLG to be named R peaks, with a subscript index giving the actual phonon branch that originates the specific band. For example, the previously named R and R′ peaks [22] will be named $\mathrm{R_{TO}}$ and $\mathrm{R_{LO}}$ peaks, respectively. A low frequency family highlighted by different symbols (□) in Fig. 8(a, b) will be named $\mathrm{R_{ZO'}}$, since these peaks come from the

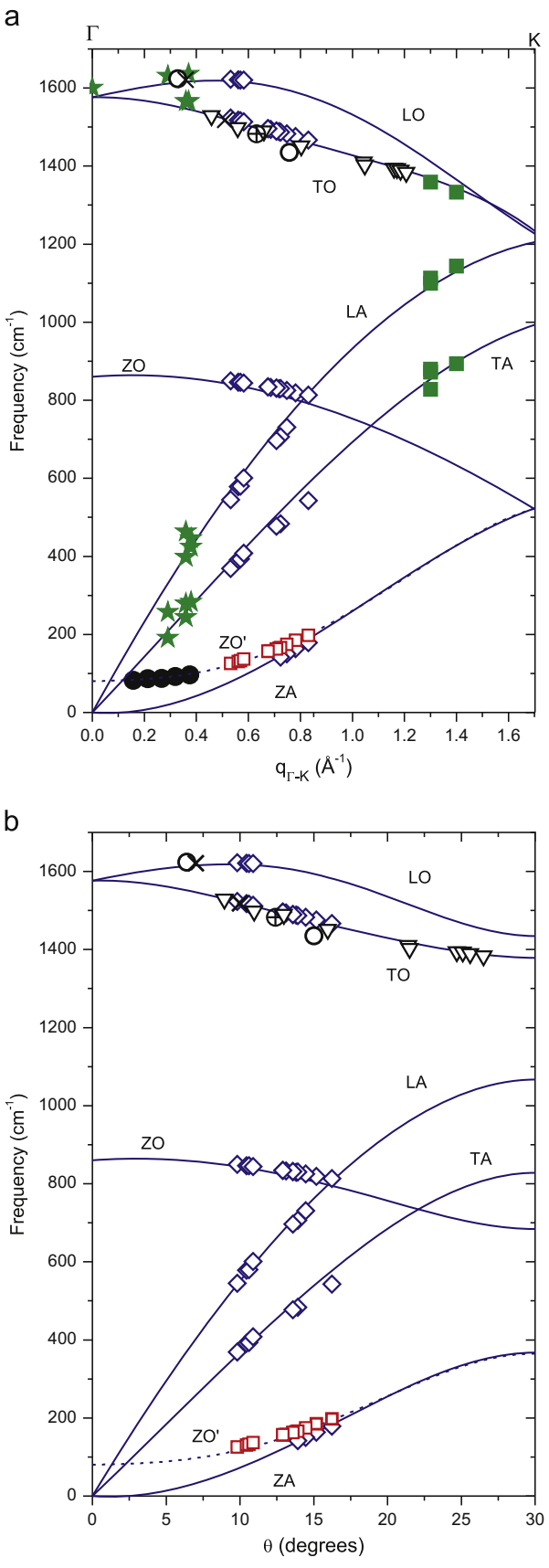

Fig. 8. (Color online) (a) Solid lines stand for the phonon frequencies (branch assignment near each curve) as a function of $q_{\Gamma-\mathrm{K}}$, taken from Ref. [31]. ◇ and □ symbols correspond to the frequencies of the rotationally induced ∗ peaks shown in Fig. 5 [12]. The • symbols are experimental data obtained from Ref. [11], where each data point was obtained using a different value of excitation laser energy. The ⋆ and ■ symbols are experimental data obtained for intravalley and intervalley double-resonance Raman processes in monolayer graphene, respectively [20]. (b) Similar plot as in (a), but with $q_{\Gamma-\mathrm{K}}$ translated to θ according to Eq. (7). The ○, ×, ⊕, and ▽ symbols in (a) and (b) are experimental data obtained from Refs. [22,6,24,25], respectively, where θ was independently determined by microscopy methods (high-resolution transmission electron microscopy [6,24,25], scanning tunneling microscopy [25] and lattice resolution atomic force microscopy [22]).

layer-breathing mode vibrations (namely ZO′ mode) occurring in bi-layer graphene, multi-layer graphene, and graphite.

The ○, ×, ⊕, and ▽ symbols in Fig. 8(a, b) are experimental data obtained from Refs. [22,6,24,25], respectively, where θ was independently determined by microscopy methods (high-resolution transmission electron microscopy [6,24,25], scanning tunneling microscopy [25] and lattice resolution AFM [22]). The $q_{\Gamma-K}$ to θ relation has been, therefore, confirmed by independent microscopy analysis.

For the second-order Raman scattering, the 2D band (also named G′ band in the literature) is a Raman allowed overtone of the so-called D band, the later being activated only in the presence of defects in the crystalline structure of graphene-related systems [13,14,18,19,32]. The 2D band frequency in graphene-based systems depends on the excitation laser energy, being very sensitive to small changes in the electronic and phonon band-structure, all due to multiple internal resonances in the electron–phonon scattering processes. Souza Filho et al. [33,34] demonstrated how this second-order Raman peak could be used to provide information about changes in the electronic structure of different (n, m) single-wall carbon nanotubes, and Ferrari et al. [35] used the same concept to show that Raman spectroscopy could be applied to determine the number of layers in an AB-stacked graphene sample.

For tBLG, Kim et al. [6] studied the 2D band Raman spectra dependence on θ [see Fig. 9(a)]. They fitted the spectra with a single Lorentzian curve for simplicity and showed that the Lorentzian full width at half maximum (FWHM) [Fig. 9(b)], central frequency [Fig. 9(c)] and integrated area [Fig. 9(d)] change dramatically with changing θ. The complex 2D band behavior was successfully modeled [red circles in Fig. 9(b–d)] by considering the θ dependent changes in the tBLG electronic structure, making use of the multiple-resonance model previously applied to carbon nanotubes [33,34] and AB-stacked N-layers graphene [35]. The non-monotonic behavior observed for the 2D peak happens when θ achieves a critical angle for which the tBLG θ-dependent van Hove singularity matches the excitation laser energy ($E_{vHs} \sim E_L$). Analogously, a non-monotonic behavior can be observed for a given θ by changing E_L, as shown in Ref. [7] for tBLG, or previously for carbon nanotubes [33]. The E_L dependence of the Raman intensities will be discussed in Section 6.

5. Comparison with the double-resonance Raman processes in graphitic materials

The ⋆ and ■ symbols in Fig. 8(a) are experimental Raman data obtained from graphene [20], and located in the phonon dispersion using the broadly studied intravalley (near Γ point) and intervalley (near K point) double-resonance (DR) Raman processes in graphitic materials [13,14,18,19,32]. This DR Raman process has been used to map the phonon dispersion of graphitic materials, but it differs from the process in tBLG in many ways: (1) The intravalley DR Raman processes probe phonons near the Γ point; the intervalley DR Raman processes probe phonons near the K point. The new R bands [see Fig. 8(a)] cover the lack of experimental data left by the usual DR Raman processes, and these two techniques complement each other for probing the vibrational spectrum of graphene systems. (2) In tBLG $\mathbf{q}(\theta)$ is a θ-defined wavevector, including its direction, while in DR Raman, averages of $\mathbf{q}$ values around the high symmetry Γ and K points apply. (3) In the DR Raman, the different phonon wavevectors $\mathbf{q}$ are probed by changing the excitation laser energy, thus changing the double resonance condition. In tBLG, the phonon wavevectors $\mathbf{q}(\theta)$ in the

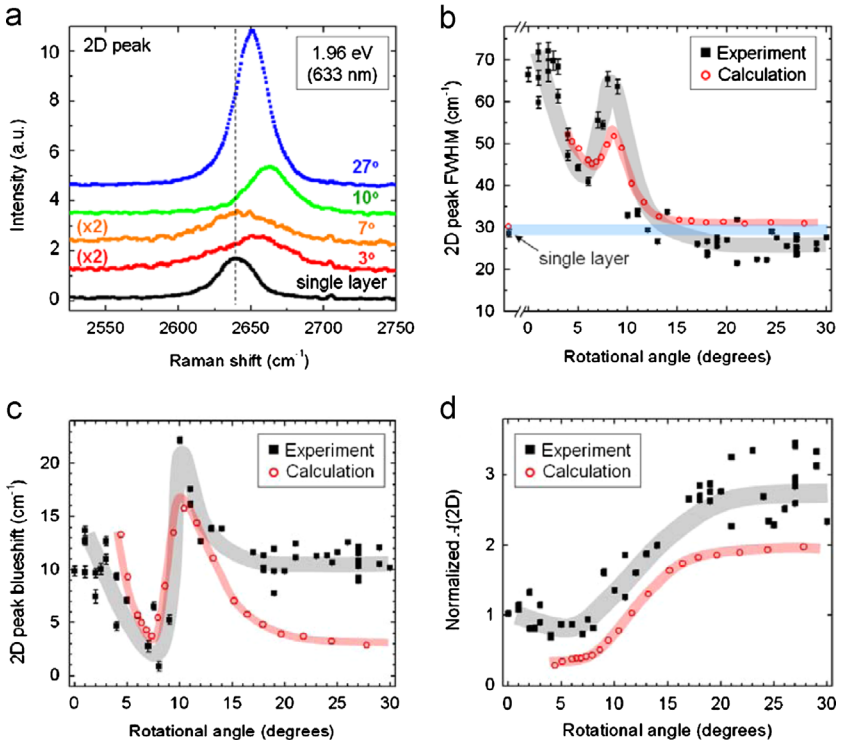

Fig. 9. (Color online) (a) 2D (or G′) band spectra for tBLG with different θ, as displayed next to the respective spectrum. The vertical dashed line represents the 2D frequency for single-layer graphene (bottom spectrum). (b) FWHM, (c) frequency blue-shift with respect to the value from single-layer graphene, and (d) integrated area for the Lorentzian peak used to fit the 2D peak. The black squares and red circles are the experimental and theoretical calculation values. The blue line in (b) indicates the single-layer graphene value. The gray (experiment) and red (calculation) areas are guides to the eye. In (d), experimental and calculation values were normalized to the single-layer value. From Ref. [6].

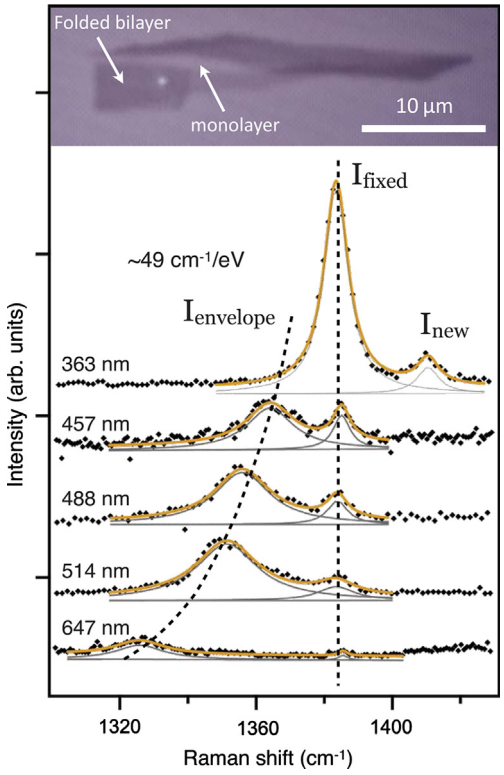

Fig. 10. (Color online) Raman spectra of tBLG in the range of 1300–1400 cm^{-1}, measured with different excitation lasers, with wavelengths 363, 457, 488, 514, and 647 nm, as displayed near the respective spectrum. The inset at the top shows an optical image of the sample. From Ref. [27].

interior of the Brillouin zone are spanned without changing the excitation laser energy, but changing the twisting angle θ. (4) The first-order R band scattering is activated in tBLG by the superlattice modulation, without requiring defects to break the $q\sim 0$ Raman selection rule. In the usual DR Raman, defects are needed to activate the first-order Raman scattering. Alternatively, the DR enhances Raman allowed phonon combinations and overtones.

Fig. 10 [27] illustrates some of the differences listed above. While the D band (labeled $I_{envelop}$ in Fig. 10) is dispersive (frequency changes with changing excitation laser energy), the R peak is not (labeled I_{fixed} in Fig. 10). The D and R bands also exhibit different intensity behaviors (see Section 6 for more information about the intensity behavior). Interestingly, the superlattice potential in tBLG was shown to be able to activate the D band generated by long-range defects, such as Coulomb impurities, intercalants, or strain [7]. Therefore, the presence of a superlattice allows the use of Raman spectroscopy to investigate a class of defects in graphene-type samples that are hardly accessible otherwise [36].

As another example, the overtone 2ZO′ has been recently observed for few-layer graphenes (from two to six layers) and graphite by the DR Raman technique [11]. The • symbols in Fig. 8(a) are the experimental data obtained from Ref. [11], where each data point was obtained using a different value of excitation laser energy. In tBLG the ZO′ phonons (□ symbols in Fig. 8) are observed in a first-order scattering process, and its observation through the $R_{ZO'}$ peak reveals the interaction between the two rotationally stacked planes. Deeper explorations can provide accurate experimental information for the development of theoretical models for the phonon dispersion in tBLG, including the coupling between layers in this system which has no AA nor AB stacking.

6. The E_L dependence of the Raman intensities—resonances and van Hove singularities

Because graphene is a zero gap semiconductor, Raman scattering in graphene is always a resonant process. Due to the smooth and (quasi)linear dispersion of the π bands from the Fermi level up to the visible light energy range, resonance effects are not evidenced like in carbon nanotubes or other semiconductor systems. However, in the case of tBLG, the presence of vHS's change this picture, and Raman spectroscopy with different excitation laser lines can be used to probe E_{vHs}. These resonances, together with theoretical calculations of the optical property of tBLG, have been used to monitor the θ-dependence of E_{vHs}, providing the result [7]

$$E_{vHs} = E_0|\sin(3\theta)|, \tag{8}$$

with E_0=3.9 eV. The maximum energy absorption occurs exactly at $\theta = 30^\circ$, for which the largest possible separation between Dirac points occurs. The E_{vHs} is expected to be symmetrical around $\theta = 30^\circ$ and periodic at 60°.

Recent theoretical and experimental works have reported the presence of such van Hove singularities in the density of π electron states in tBLG [5,37–39]. Refs. [6,7,24,40,41] have demonstrated that these vHs's induce very strong enhancement in the G band intensity, and that the maximum enhancement occurs for specific incident laser energies (E_L) defined by the twist angle θ. Fig. 11(a, b) shows, respectively, the G and R_{TO} bands obtained from the same tBLG, for six different values of E_L (1.96, 2.33, 2.41, 2.54, 2.71, and 3.84 eV). These two plots clearly show that not only the G, but also the R_{TO} band intensity presents strong dependence on E_L, the maximum enhancement occurring at the same laser energy [7].

The G band resonance effect in tBLG is described by third order time-dependent perturbation [41]. The major contribution for the intensity comes from resonance matching, that is, for $E_L = E_{vHs}$ and $E_L = E_{vHs} \pm \hbar\omega_G$, where $\hbar\omega_G$ is the energy of the G phonon, and the + and the − signs stand for the Stokes and anti-Stokes processes, respectively. Therefore, the E_L dependence of the normalized G band Stokes resonance profile shown in Fig. 11(a) can be evaluated as [7,13]

$$\frac{I(G)}{I(G_{SLG})} = \left|\frac{M}{(E_L - E_{vHs} - i\gamma)(E_L - E_{vHs} - \hbar\omega_G - i\gamma)}\right|^2, \tag{9}$$

where M is a constant that encompasses the product of the matrix elements for electron–photon and electron–phonon interactions and γ is the resonance window width, that is, the energy uncertainty related to the lifetime of the excited states. The G band intensities extracted from the data depicted in Fig. 11(a) were fitted according to Eq. (9), and the parameters E_{vHs}=2.79 eV and $\gamma = 0.12$ eV were found [7].

A similar procedure can be used to fit the R_{TO} resonance profile shown in Fig. 11(b), and the same values for E_{vHs} and γ were obtained [7]. However, the complete analysis of the R peak resonances is more complex. The R band intensity can be described by fourth-order time-dependent perturbation process in graphene, involving an additional interaction between the photo-excited electron (with wavevector $\mathbf{k}$) and the periodic potential of the superlattice (with associated wavevector $\mathbf{q}$) [41]. In this case, the normalized R band intensity is given as [7]

$$\frac{I(R)}{I(G_{SLG})} = \left|\frac{M'}{(E_L - E_{vHs} - i\gamma)[E_L - E_{eh}(\mathbf{k}+\mathbf{q}) - i\gamma](E_L - E_{vHs} - \hbar\omega_R - i\gamma)}\right|^2. \tag{10}$$

The major difference between Eqs. (9) and (10) is the new term inside the square brackets in Eq. (10), where $E_{eh}(\mathbf{k}+\mathbf{q})$ is the electron–hole pair state energy at $(\mathbf{k}+\mathbf{q})$. For the R_{TO} resonance shown in Fig. 11(b), within the measured excitation energy range,

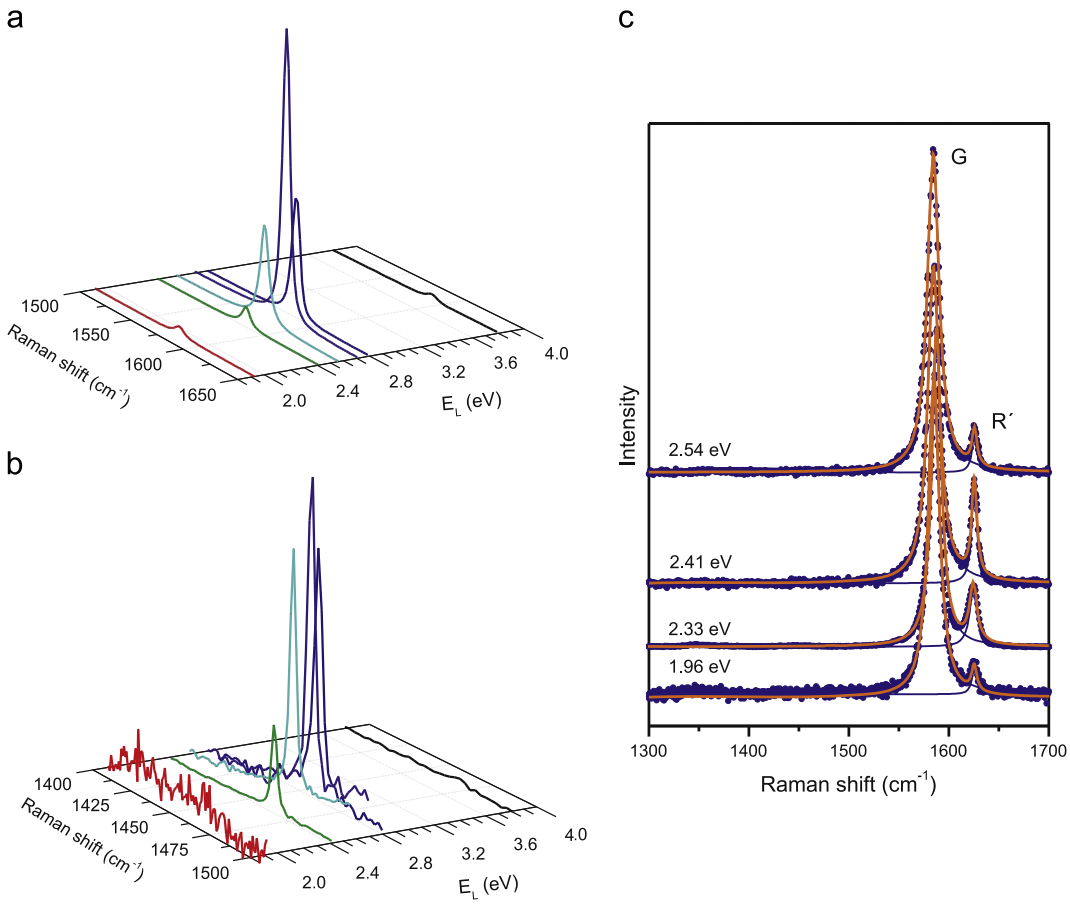

Fig. 11. (Color online) (a) and (b) show the Raman spectra obtained from a tBLG with $\theta = 13 \pm 3^{\circ}$, according to lattice-resolution AFM measurements. The (a) G and (b) R_{TO} bands exhibit similar resonance behavior. The data were normalized with respect to the G band Raman spectra of a nearby single layer graphene [7]. (c) Raman spectra of another tBLG with $\theta \simeq 6^{\circ}$, using four different excitation laser energies: $E_L = 1.96$, 2.33, 2.41, and 2.54 eV. The spectra here are normalized to the G band in the tBLG itself, and the R_{LO} Raman peak centered at 1625 cm^{-1} exhibits an extra intensity enhancement near 2.41 eV [22], due to the DR Raman effect. From Refs. [7,22].

the term between brackets in the denominator of Eq. (10) plays a minor role, because it is a smooth function of E_L, E_L being far from $E_{eh}(\mathbf{k}+\mathbf{q})$. This is why this term can be disregarded in the fitting.

However, when E_L reaches $E_{eh}(\mathbf{k}+\mathbf{q})$, intravalley or intervalley double-resonance processes can take place in the Raman scattering of tBLG as well, giving rise to extra enhancement in the R peak intensities. The E_L dependence for these two double-resonance conditions, considering for illustration a linear electronic dispersion $E(k)$, is given by [22]

$$E_L^{\text{intra}} = \hbar v_F \frac{8\pi}{\sqrt{3}a} \sin\left(\frac{\theta}{2}\right), \tag{11}$$

and

$$E_L^{\text{inter}} = \hbar v_F \frac{4\pi}{3a} \sqrt{12 \sin^2\left(\frac{\theta}{2}\right) - 2\sqrt{3}\sin\theta + 1}, \tag{12}$$

where v_F is the Fermi velocity in graphene ($\sim 10^6$ m/s). Fig. 12(a, b) shows the plot of E_L^{intra} and E_L^{inter} as a function of θ. Notice that the condition for intervalley double-resonance Raman process [Fig. 12(b)] would only be achieved for excitation laser energies in the UV range. However, intravalley double-resonance Raman processes [Fig. 12(a)] can be achieved for excitation laser energies in the infrared and visible range. Corrections are needed due to the departure from the linear $E(k)$ relation for energies near 3eV and higher.

This phenomenon is shown in Fig. 11(c), where the Raman spectra from another tBLG were measured using four different excitation laser energies: $E_L = 1.96$, 2.33, 2.41, and 2.54 eV. The R_{LO} peak centered at ~ 1625 cm^{-1} presents a higher intensity for the spectrum obtained using $E_L = 2.41$ eV. Here the spectra are normalized to the G band in tBLG itself, thus showing an extra resonance phenomenon for the R_{LO} band. This sample was inspected by lattice-resolution AFM, and the measurements revealed a $\theta \simeq 6^{\circ}$. The green bullet in Fig. 12(a) indicates that this experimental data is in good agreement with the theoretical predictions.

Finally, Sato et al. [41] performed extensive zone folding calculations based on a definition of the tBLG unit cell with indices (n, m) [see Fig. 13(a)]. They predict the observation of a more complex picture of possible transitions, including more than one van Hove singularity in the joint density of states (JDOS) for a given tBLG [see Fig. 13(b)] and a rich dependence of the JDOS peaks on mod$(n-m, 3)$ [see Fig. 13(c)]. The E_{vHs} dependence on tBLG structure can be consistently reorganized when plotting the JDOS peaks as a function of the lattice constant T [see Fig. 13(d)], although more than one optical transition is still predicted.

7. Final remarks

In this paper we briefly discussed the structure and production of twisted bi-layer graphene (tBLG). This system represents a prototype material for a two-dimensional Moiré type superstructure, where interesting effects caused by the presence of a periodic superlattice modulation can be probed using microscopy and spectroscopy. Here we focused mostly on the use of resonance Raman spectroscopy to study and characterize the tBLG electronic and vibrational properties.

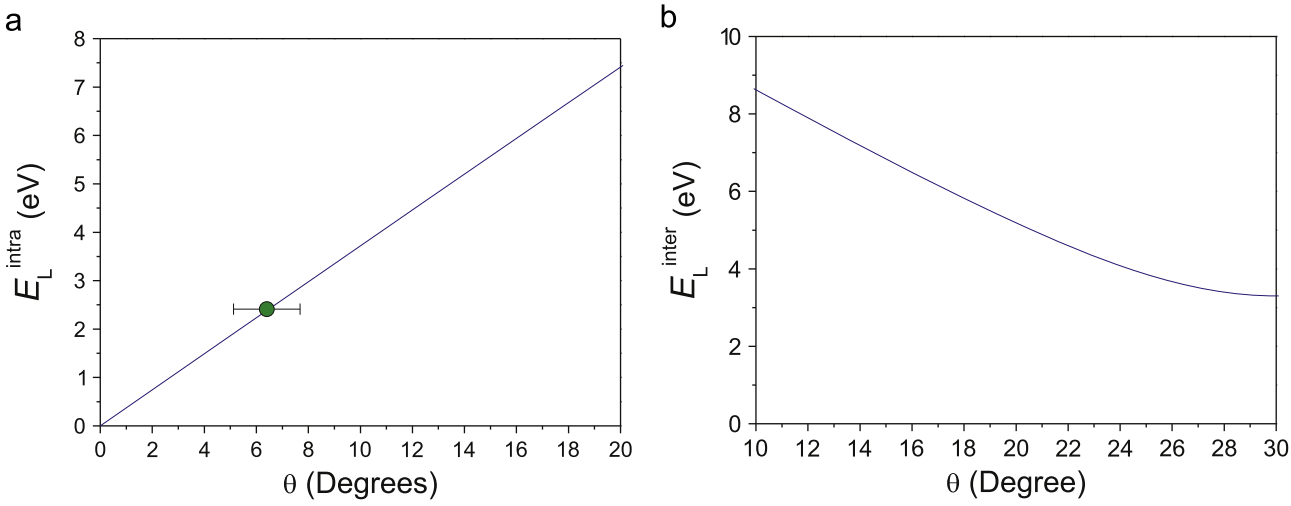

Fig. 12. (Color online) (a) Plot of E_L^{intra} as a function of θ, according to Eq. (11). (b) Plot of E_L^{inter} as a function of θ, according to Eq. (12). The green circle in panel (a) is the plot of the experimental data depicted in Fig. 11(c) ($\omega_{R_{LO}} = 1625\ cm^{-1}$ and E_L^{intra}=2.41 eV), obtained from the Raman spectra of a tBLG with $\theta \simeq 6^\circ$. The error bar indicates the uncertainty in the determination of θ. From Ref. [22].

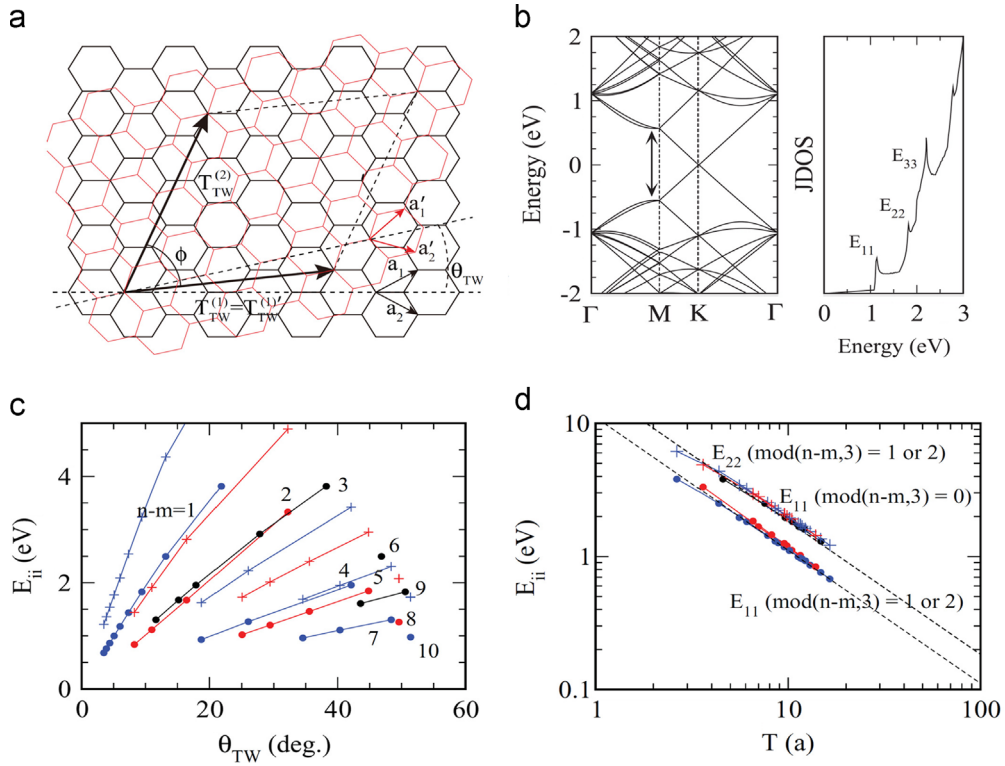

Fig. 13. (Color online) (a) The unit cell for a tBLG, defined by the indices $(n,m) = (3,2)$, as introduced by Sato et al. [41]. The second graphene layer (red) is rotated by $\theta = 13.17^\circ$ relative to the AB stacking (notice that the authors use θ_{TW} in their paper). (b) The energy bands (left) and the joint density of states (JDOS) (right) for the (7,5), showing three van Hove singularities E_{vHs}. (c) E_{vHs} as a function of the twisted angle θ (or θ_{TW}) of the tBLG. The data points for each family $n - m =$ const are connected by a line. The black, blue, and red symbols are mod$(n-m,3) = 0$, mod$(n-m,3) = 1$, and mod$(n-m,3) = 2$, respectively. The circle and plus symbols denote E_{vHs}=E_{11} and E_{22}, respectively. (d) E_{vHs} as a function of the lattice constant T of tBLG on a log–log scale. Each family $n-m =$ constant is connected by a line. Colors and symbols are the same as in (c). From Ref. [41].

The resonance Raman effects are especially rich in this system, where both resonances with van Hove singularities, as previously observed in carbon nanotubes, as well as multiple-resonance processes, as largely studied in graphitic structures, take place. We here put all these effects together, in a fully consistent picture.

Besides the application of the knowledge presented here as a characterization tool for the development of tBLG-based science and technology, several aspects still remain to be studied using Raman spectroscopy. Two aspects that urge work are (1) the observation of the predictions by Sato et al. [41] with respect to the rich dependence of the optical transition energies on the tBLG structure, and (2) the possibility of studying long-range defects, such as Coulomb impurities, intercalants, or strain [7].

The tBLG is also a prototype for studying the interlayer interactions. The Raman spectroscopy results presented here show that this system exhibits the inter-layer breathing modes (named ZO′ phonon branch), that can now be studied accurately, even in the absence of the usual AB stacking.

One last important aspect is the sharp linewidth for the superlattice induced peaks, unusual in graphene. The R peaks can exhibit full width at half maximum (FWHM) as narrow as $\Gamma_R \approx 4\,cm^{-1}$, indicating when the $\mathbf{q}(\theta)$ wavevector is very well defined. Coupled to the strong θ-dependence of the R frequencies, it turns out that measuring $\Gamma_R \approx 4\,cm^{-1}$ provides a straightforward test for tBLG structural homogeneity, which might be important for researchers exploring the science and application of these structures.

Acknowledgments

The authors acknowledge discussion with Prof. R. Saito and Prof. Rodrigo B. Capaz. This work was financed by CNPq (473840/2012-0, 552124/2011-7 and 551953/2011-0 Grants), FAPEMIG and Inmetro. L.G.C. acknowledges the Grant PRONAMETRO (52600.056330/2012).

References

[1] W.-T. Pong, C. Durkan, Journal of Physics D: Applied Physics 38 (2005) R329.
[2] K.S. Novoselov, A.K. Geim, S.V. Morozov, D. Jiang, Y. Zhang, S.V. Dubonos, I.V. Grigorieva, A.A. Firsov, Science 306 (2004) 666.
[3] E.J. Mele, Physical Review B 81 (2010) 161405.
[4] E.S. Morell, J.D. Correa, P. Vargas, M. Pacheco, Z. Barticevic, Physical Review B 82 (2010) R121407.
[5] G. Li, A. Luican, J.M.B. Lopes dos Santos, A.H. Castro Neto, A. Reina, J. Kong, E.Y. Andrei, Nature Physics 6 (2) (2010) 109.
[6] K. Kim, S. Coh, L.Z. Tan, W. Regan, J.M. Yuk, E. Chatterjee, M.F. Crommie, M.L. Cohen, S.G. Louie, A. Zettl, Physical Review Letters 108 (2012) 246103.
[7] V. Carozo, C.M. Almeida, B. Fragneaud, P. Bedê, J. Moutinho, M.V.O. Ribeiro-Soares, N. Andrade, A.G. Souza Filho, M.J.S. Matos, B. Wang, M. Terrones, R.B. Capaz, A. Jorio, C.A. Achete, L.G. Cançado, Resonance effects on the Raman spectra of graphene superlattices, Physical Review B 88 (2013) 085401.
[8] G.T. Laissardiére, D. Mayou, L. Mangaud, Nano Letters 10 (2010) 804.
[9] J.T. Robinson, S.W.C. Schmucker, B. Diaconescu, J.P. Long, J.C. Culbertson, T. Ohta, A.L. Friedman, T.E. Beechem, ACS Nano 7 (2013) 637–644.
[10] J. Campos-Delgado, G. Algara-Siller, U. Kaiser, J.-P. Raskin, Twisted bi-layer graphene: microscopic rainbows, Small 9 (19) (2013) 3247–3251.
[11] C.H. Lui, L.M. Malard, S.H. Kim, G. Lantz, F.E. Leverge, R. Saito, T. Heinz, Nano Letters 12 (2012) 5539.
[12] J. Campos-Delgado, L.G. Cançado, C.A. Achete, A. Jorio, J.-P. Raskin, Nano Research 6 (4) (2013) 269–274.
[13] A. Jorio, M.S. Dresselhaus, R. Saito, G. Dresselhaus, Raman Spectroscopy in Graphene Related Systems, Wiley-VCH, 2011.
[14] R. Saito, M. Hofmann, G. Dresselhaus, A. Jorio, M.S. Dresselhaus, Advances in Physics 60 (2011) 413.
[15] A. Jorio, R. Saito, J.H. Hafner, C.M. Lieber, M. Hunter, T. McClure, G. Dresselhaus, M.S. Dresselhaus, Physical Review Letters 86 (6) (2001) 1118.
[16] C. Fantini, A. Jorio, M. Souza, M.S. Strano, M.S. Dresselhaus, M.A. Pimenta, Physical Review Letters 93 (14) (2004) 147406.
[17] H. Telg, J. Maultzsch, S. Reich, F. Hennrich, C. Thomsen, Physical Review Letters 93 (17) (2004) 177401.
[18] R. Saito, A. Jorio, A.G. Souza Filho, G. Dresselhaus, M.S. Dresselhaus, M.A. Pimenta, Physical Review Letters 88 (2001) 027401–027404.
[19] S. Reich, C. Thomsen, Philosophical Transactions of the Royal Society of London. Series A: Mathematical, Physical and Engineering Sciences 362 (1824) (2004) 2271–2288.
[20] S. Bernard, E. Whiteway, D.G. Yu, V. Austing, M. Hilke, Physical Review B 86 (2012) 085409.
[21] M.A. Bissett, W. Izumida, R. Saito, H. Ago, ACS Nano 6 (11) (2012) 10229–10238.
[22] V. Carozo, C.M. Almeida, E.H.M. Ferreira, L.G. Cançado, C.A. Achete, A. Jorio, Nano Letters 11 (11) (2011) 4527.
[23] D.L. Miller, K.D. Kubista, G.M. Rutter, M. Ruan, W.A. de Heer, P.N. First, J.A. Stroscio, Physical Review B 81 (2010) 125427.
[24] R.W. Havener, H. Zhuang, L. Brown, R.G. Hennig, J. Park, Nano Letters 12 (2012) 3162.
[25] Y. Wang, Z. Su, W. Wu, S. Nie, N. Xie, H. Gong, Y. Guo, J.H. Lee, X. Xing, S. Lu, H. Wang, X. Lu, K. McCarty, F. Pei, S. Robles-Hernandez, V.G. Hadjiev, J. Bao, Twisted bilayer graphene superlattices, arXiv:1301.4488v1.
[26] C.M. Almeida, V. Carozo, R. Prioli, C.A. Achete, Journal of Applied Physics 110 (2011) 086101.
[27] A.K. Gupta, Y. Tang, V.H. Crespi, P.C. Eklund, Physical Review B 82 (2010) 241406.
[28] A.T. N'Diaye, J. Coraux, T.N. Plasa, C. Busse, T. Michely, New Journal of Physics 10 (2008) 043033.
[29] P. Poncharal, A. Ayari, J.L. Michel, T. Sauvajol, Physical Review B 78 (2008) 113407.
[30] Z. Ni, T.S.Z. Wang, Y. Yu, Nano Research 1 (2008) 273.
[31] P. Venezuela, M. Lazzeri, F. Mauri, Physical Review B 84 (2011) 035433.
[32] C. Thomsen, S. Reich, Physical Review Letters 85 (2000) 5214–5217.
[33] A.G. Souza Filho, A. Jorio, G. Dresselhaus, M.S. Dresselhaus, R. Saito, A.K. Swan, M.S. Unlu, B.B. Goldberg, J.H. Hafner, C.M. Lieber, M.A. Pimenta, Physical Review B 65 (2001) 035404.
[34] A.G. Souza Filho, A. Jorio, A.K. Swan, M.S. Unlu, B.B. Goldberg, R. Saito, J.H. Hafner, C.M. Lieber, M.A. Pimenta, G. Dresselhaus, M.S. Dresselhaus, Physical Review B 65 (2002) 085417–085424.
[35] A.C. Ferrari, J.C. Meyer, V. Scardaci, C. Casiraghi, M. Lazzeri, F. Mauri, S. Piscanec, D. Jiang, K.S. Novoselov, S. Roth, A.K. Geim, Physical Review Letters 97 (18) (2006) 187401.
[36] A. Eckmann, A. Felten, A. Mishchenko, L. Britnell, R. Krupke, K.S. Novoselov, C. Casiraghi, Nano Letters 12 (8) (2012) 3925–3930.
[37] J.M.B. Lopes dos Santos, N.M.R. Peres, A.H. Castro Neto, Physical Review Letters 99 (2007) 256802.
[38] T. Ohta, J.T. Robinson, P.J. Feibelman, A. Bostwick, E. Rotenberg, T.E. Beechem, Physical Review Letters 109 (2012) 186807.
[39] I. Brihuega, P. Mallet, H. Gonzalez-Herrero, G. Trambly de Laissardiere, M.M. Ugeda, L. Magaud, J.M. Gomez-Rodriguez, F. Yndurain, J.-Y. Veuillen, Physical Review Letters 109 (2012) 196802.
[40] Z. Ni, L. Liu, Y. Wang, Z. Zheng, L.-J. Li, T. Yu, Z. Shen, Physical Review B 80 (2009) 125404.
[41] K. Sato, R. Saito, C. Cong, T. Yu, M.S. Dresselhaus, Physical Review B 86 (2012) 125414.